Electronic Supplementary Material (ESI) for Journal of Materials Chemistry A.
This journal is © The Royal Society of Chemistry 2022

Electronic Supplementary Information

Two-dimensional Covalent Organic Frameworks with Double Redox-Active Centers for Organic High-performance Li-ion Batteries Cathode

Lei Gong, Xiya Yang, Ying Gao, Gengxiang Yang, Zonghua Yu, Xianzhang Fu, Yinhai Wang, Dongdong Qi, Yongzhong Bian, Kang Wang, and Jianzhuang Jiang

Beijing Key Laboratory for Science and Application of Functional Molecular and Crystalline Materials, Department of Chemistry, School of Chemistry and Biological Engineering, University of Science and Technology Beijing, Beijing 100083, China

Daxing Research Institute, and Beijing Advanced Innovation Center for Materials Genome Engineering, University of Science and Technology Beijing, Beijing 100083, China

Contents

1 Experimental section.

2 Fig. S1. FT-IR spectra of TPPDA-CuPor-COF.

3 Fig. S2. High-resolution XPS spectra of TPPDA-CuPor-COF.

4 Fig. S3. The solid state diffuse reflectance electronic absorption spectra of TPPDA-CuPor-COF.

5 Fig. S4. Experimental and simulated PXRD patterns of TPPDA-CuPor-COF.

6 Fig. S5. The SEM image of TPPDA-CuPor-COF.

7 Fig. S6. EDS mapping images of TPPDA-CuPor-COF.

8 Fig. S7. TG curve of TPPDA-CuPor-COF.

9 Fig. S8. PXRD patterns of TPPDA-CuPor-COF soaked in different solutions.

10 Fig. S9. Cycling performance at different voltage ranges of TPPDA-CuPor-COF.

11 Fig. S10. The average output voltages at different voltage ranges of TPPDA-CuPor-COF.

12 Fig. S11. Energy densities of TPPDA-CuPor-COF under different voltage ranges.

13 Fig. S12. The TEM images of TPPDA-CuPor-COF cathode after charged and discharged.

14 Fig. S13. The SEM images of TPPDA-CuPor-COF cathode after 50 cycles of charge-discharge.

15 Fig. S14. The *ex*-situ XRD diagram of TPPDA-CuPor-COF cathode after 50 cycles of charge-discharge

16 Fig. S15. The CV curves at different scan rates.

17 Fig. S16. The corresponding plots of log(*i*) versus log(*v*) at each redox peak.

18 Fig. S17. CV profiles and the pseudocapacitive contributions (black shadow) at different scan rates of TPPDA-CuPor-COF.

19 Fig. S18. The Nyquist plots and simulated equivalent circuit of the electrode/electrolyte interface.

20 Fig. S19. The MESP mapping images of [TPPDA-CuPor]$^{+}$ and [TPPDA-CuPor]$^{2+}$•PF_6^-.

21 Fig. S20. The MESP mapping images of [TPPDA-CuPor]$^{3+}$•$2PF_6^-$ and [TPPDA-CuPor]$^{4+}$•$3PF_6^-$.

22 Fig. S21. The MESP mapping images of TPPDA-CuPor $^{-}$ and [TPPDA-CuPor]$^{2-}$•Li^{+}.

23 Fig. S22. The energies of the HOMO and LUMO of TPPDA-CuPor under different redox states.

24 Fig. S23. The differential charge analyses between TPPDA-CuPor and charge carriers.

25 Table S1. The ICP-OES result for the content of metal in TPPDA-CuPor-COF.

26 Table S2. Comparison of organic p- and bipolar-type cathode materials in Lithium-ion battery.

27 Table S3. The fitting parameters of EIS data.

28 References.

EXPERIMENTAL SECTION

Characterization

Powder X-ray diffraction (PXRD) was collected at room temperature on a PANalytical Empyrean series 3 diffractometer equipped with Cu K_α radiation. FT-IR spectra were recorded as KBr pellets using a Bruker Tensor 37 spectrometer with 4 cm^{-1} resolution. X-ray photoelectron spectroscopy (XPS) data were recorded on a Thermo Scientific K-Alpha system. Al K_α X-ray (6 mA / 12 KV) was utilized as the irradiation source. All XPS measurements were performed in the CAE mode with the reference of C 1s (284.8 eV). The nitrogen adsorption and desorption isotherm were measured at 77 K were measured at 298 K using a Micromeritics ASAP 2020 PLUS HD88 system. The samples were degassed at 90°C for 4 hours before the measurements. The thermogravimetric analysis (TGA) was performed on a ZRT-A thermogravimetric analyzer instrument under nitrogen atmosphere with a heating rate of 10°C/min. The metal content of TPPDA-CuPor-COF was determined by inductively coupled plasma (ICP) analysis with an Aglient 5110 ICP-OES instrument. The images of high-resolution field transmission electron microscopy (HR-TEM), high angle annular dark-field scanning transmission electron microscope (HAADF-STEM) and energy dispersive spectroscopy (EDS) mappings were collected by transmission electron microscopy (JEM-2100F) at an operation voltage of 200 kV. Scanning electron microscopy (SEM) images were obtained on a HITACHI SU8010 microscope. The transmission electron microscopy (TEM) image was acquired on HITACHI HT7700

with an electron acceleration energy of 100 kV. UV-vis diffuse reflectance absorption spectra (DRS) were recorded on a Shimadzu UV-2600 spectrophotometer with $BaSO_4$ as the reference.

Electrochemical Measurements

Electrochemical lithium-storage properties of TPPDA-CuPor-COF were measured by using CR2032 coin-type test cells assembled in argon-filled glove box (the oxygen and water concentration maintained below 1 ppm). To fabricate the working electrode, a slurry with appropriate viscosity consisting of 50wt% active materials, 40wt% Super-P carbon and 10wt % PVDF binder dissolved in NMP was casted on the Al foil, drying at 100°C under vacuum for 24 h. The loading mass of electroactive materials in electrode slurry is about 0.8 mg/cm^{-2}. Pure lithium foil was used as the counter electrode, and 1mol/L LiPF6 in EC/EMC (3:7 v/v) was served as the electrolyte, and a porous Celgard 2400 as separator. Galvanostatic charge/discharge cycles were performed in a potential range of 1.5 − 4.2 V vs. Li/Li^+ on a LAND 2001A instrument (Wuhan, China). CHI 660E electrochemical workstation (Shanghai, China) was used to record the CV and electrochemical EIS with a frequency range from 10^{-1} to 10^6 Hz.

***Ex situ* XPS measurement and sample preparation**

When conducting *ex situ* XPS measurements of TPPDA-CuPor-COF, the coin cells were cycled to charged state (4.2 V) and discharged state (1.5 V), respectively. Then the coin cells were disassembled and the obtained electrodes were washed with THF

and dried in argon-filled glove box before tests.

Structure modeling

The unit cells of the models were refined with the experimental PXRD data of TPPDA-CuPor-COF by using the Le Bail refinement. The cell parameters and the refined PXRD patterns were obtained until the values of R_{wp} and R_p converged.

Calculations of theoretical capacity, energy density and power density

Theoretical capacity C_t (mA h g^{-1}) was calculated using the following equation:[1]

$$C_t = \frac{nF}{3600(M_w/1000)}$$

Where n and M_w is the number of charge carrier and the molecular weight of the active material, respectively, F is the Faraday constant (96485 C mol^{-1}).

In the TPPDA-CuPor-COF, the molecular weight of a repeating unit ($C_{78}H_{51}N_{10}Cu$) is calculated to be M_w = 1191.88 g mol^{-1}. The number of electrons (n) involved in the repeating unit is 6. Therefore, the theoretical capacity is calculated using the equation of C_t = 134.92 mA h g^{-1}.

The energy density (E) of the electrode can be calculated based on the equation:

$E = C_{capacity} \times V_{average}$, where $C_{capacity}$ is the experimental specific capacity and $V_{average}$ is the average output potential (vs. Li/Li^+) of the electrode.

DFT calculation methods

Density functional theory (DFT) calculations were performed by B3LYP-D3

method with Becke-Johnson damping.[2,3] The def2-SVP basis set was utilized to optimize the structures of the TPPDA-CuPor-COF repeat unit and the complexes, and the def2-SVPD basis set was applied to calculate the energies using Gaussian 09 program (version D.01).[4,5] The Molecular electrostatic potential (MESP) and differential charge analysis were carried out by Multiwfn software.[6] All visualization of MESP plots are performed by the Visual Molecule Dynamics (VMD) software.[7] The differential charge density ($\Delta\rho$) was calculated by the formula:[8]

$$\Delta\rho\ (PF_6^-) = \rho(\text{TPPDA-CuPor} - x e^- + x PF_6^-) - x\rho(PF_6^-) - \rho(\text{TPPDA-CuPor}^{x+})$$

$$\Delta\rho\ (Li^+) = \rho(\text{TPPDA-CuPor} + x e^- + x Li^+) - x\rho(Li^+) - \rho(\text{TPPDA-CuPor}^{x-})$$

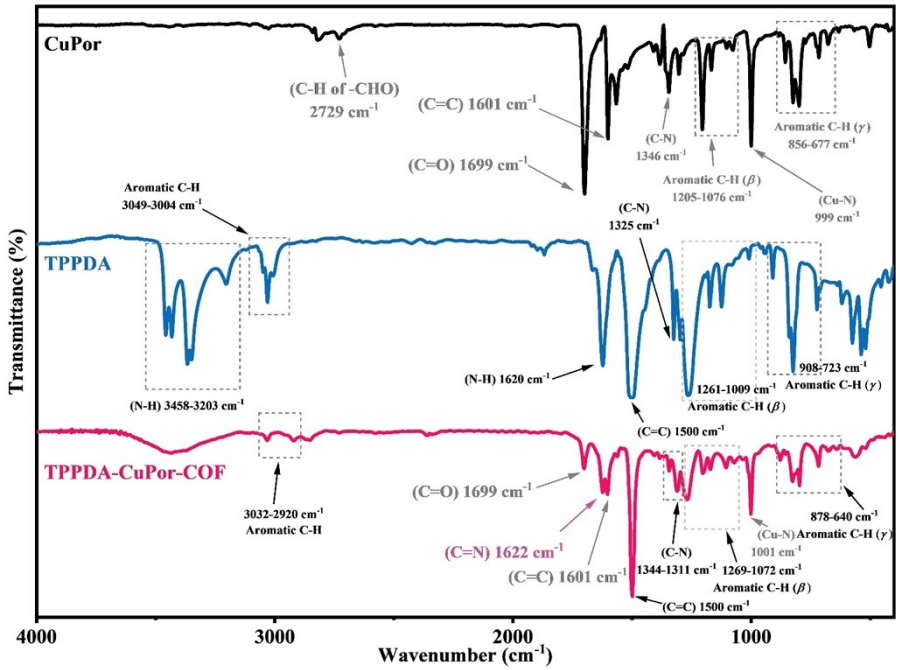

Fig. S1. FT-IR spectra of TPPDA-CuPor-COF, TPPDA and CuPor.

(Note: a. aromatic C-H (β):in-plane bending vibration; aromatic C-H (γ):out-of-plane bending vibration.)

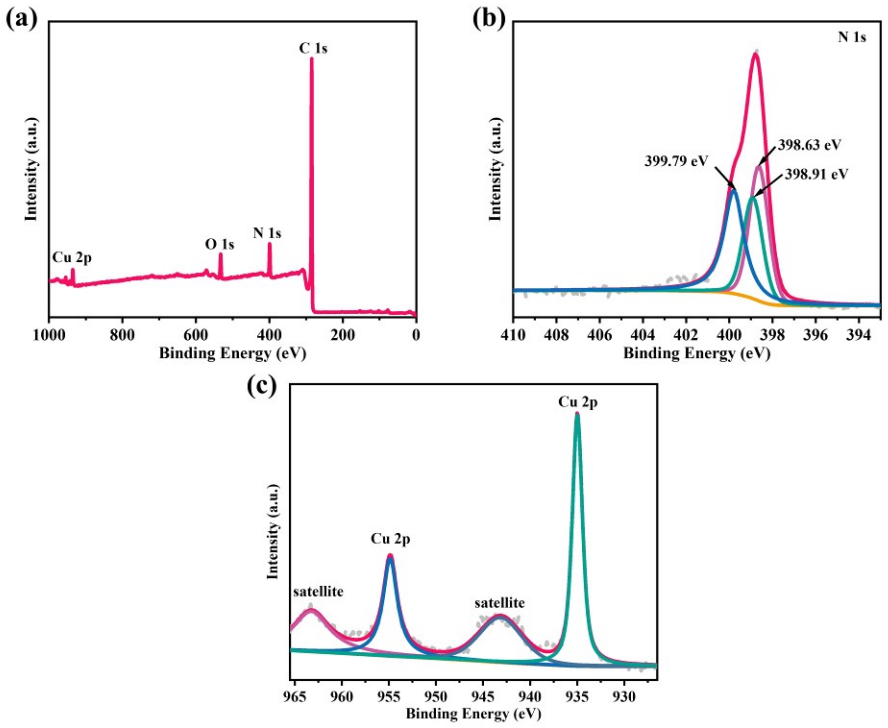

Fig. S2. High-resolution XPS spectra of TPPDA-CuPor-COF. (a) Total XPS spectrum of TPPDA-CuPor-COF. (b) High-resolution scan of N 1s. (c) High-resolution scan of Cu 2p.

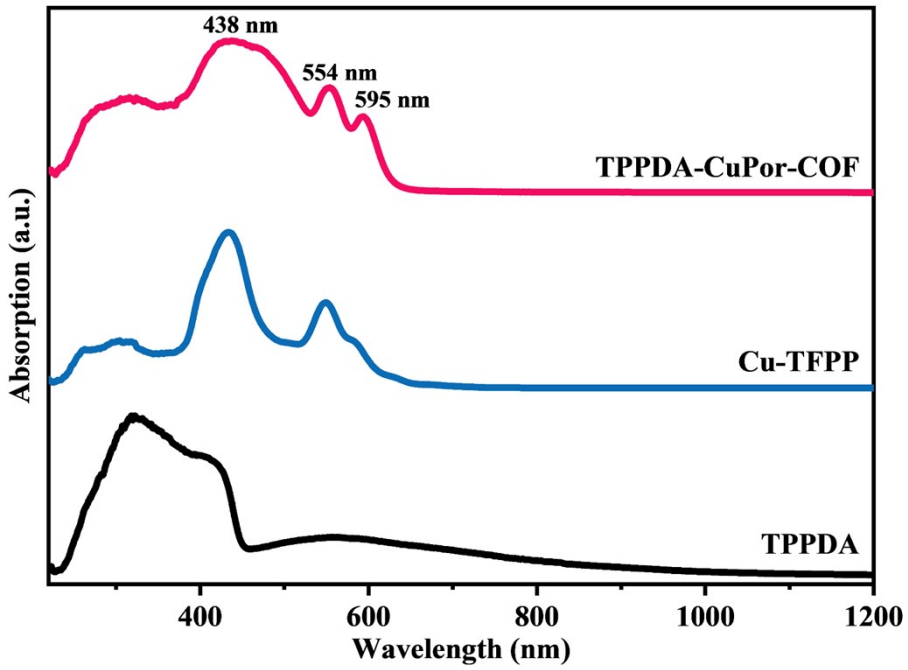

Fig. S3. The solid state diffuse reflectance electronic absorption spectrum of TPPDA-CuPor-COF, Cu-TFPP and TPPDA.

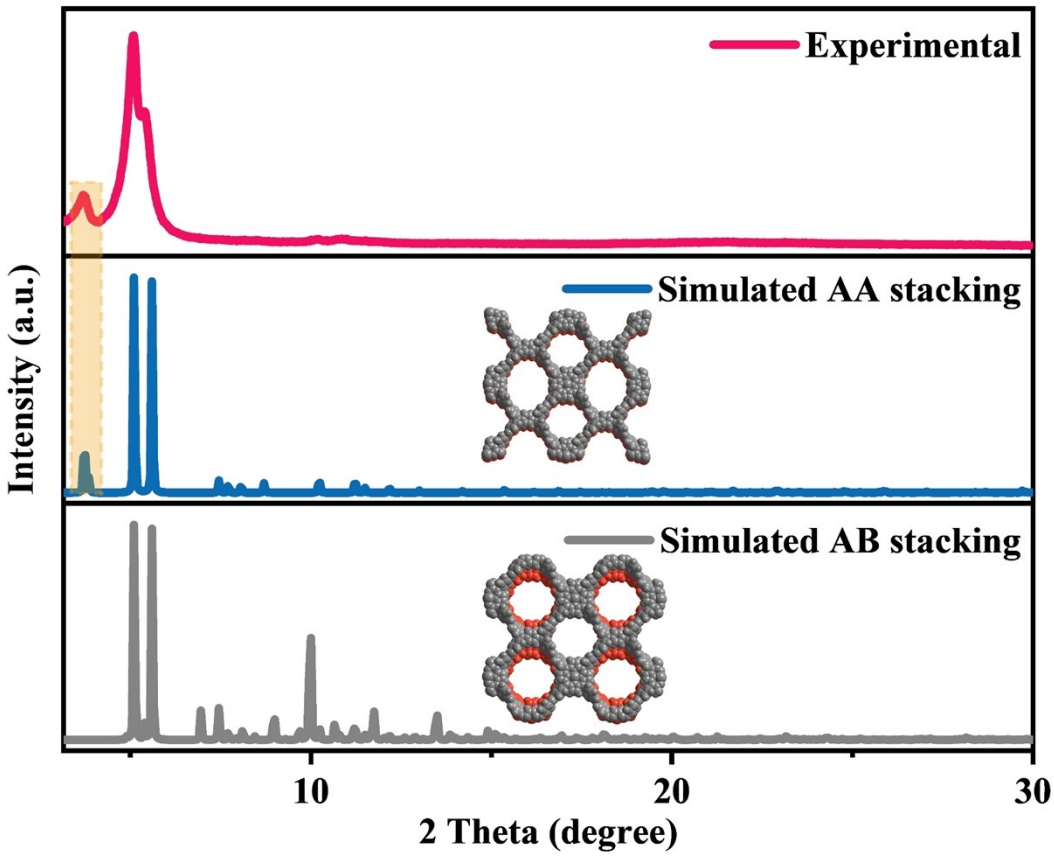

Fig. S4. Experimental and simulated (AA and AB stacking) PXRD patterns of TPPDA-CuPor-COF (The insetted molecular models are AA and AB stacking model, respectively).

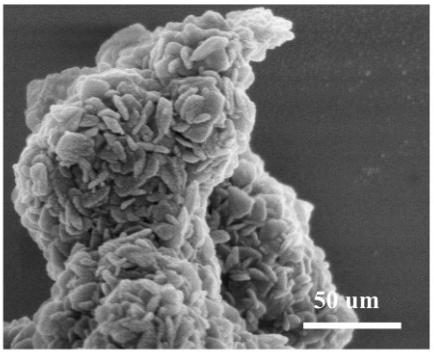

Fig. S5. The SEM image of TPPDA-CuPor-COF.

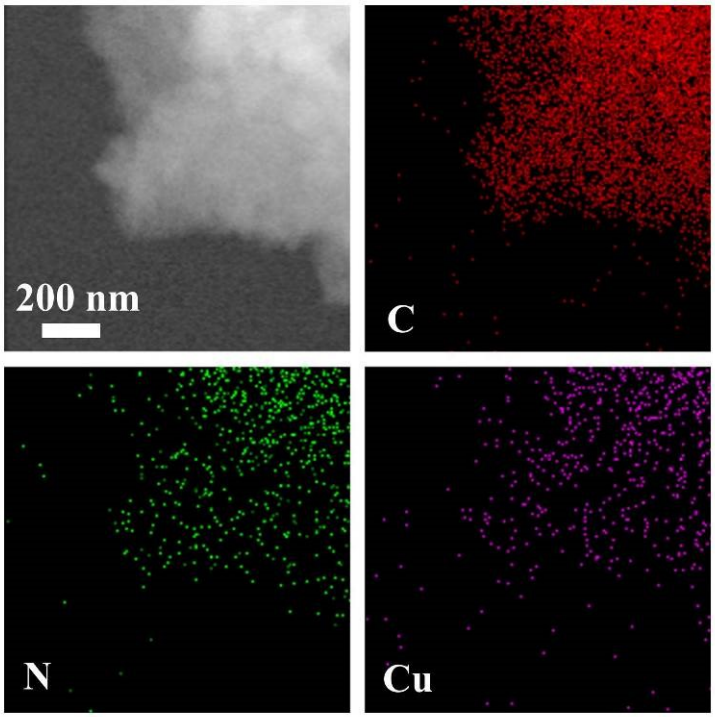

Fig. S6. EDS mapping images of TPPDA-CuPor-COF.

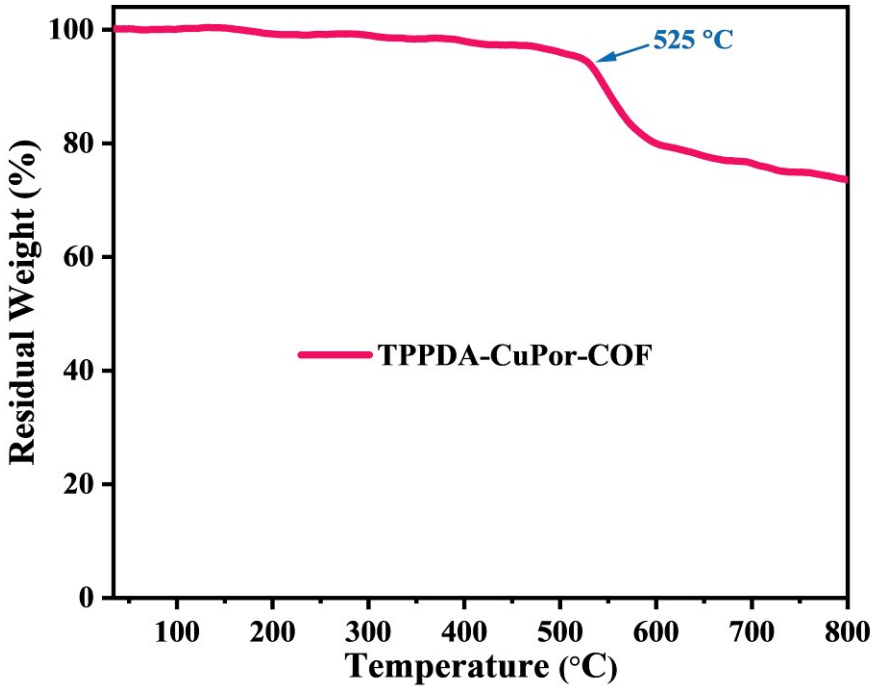

Fig. S7. The TG curve of TPPDA-CuPor-COF with a constant heating rate of 10℃ min^{-1} from 30 to 800℃ in N_2.

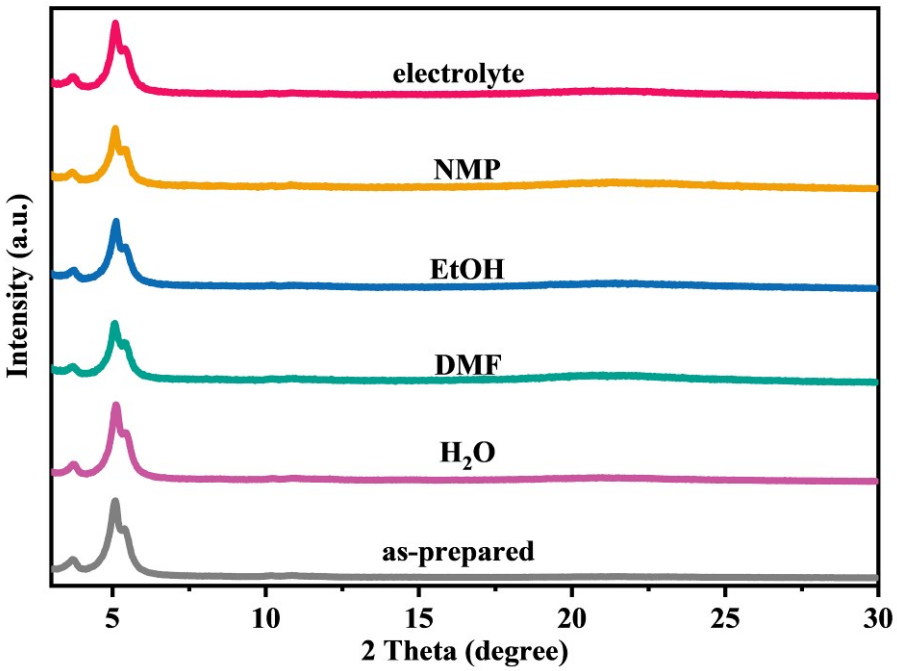

Fig. S8. PXRD patterns of TPPDA-CuPor-COF after soaking in different solutions for 7 days.

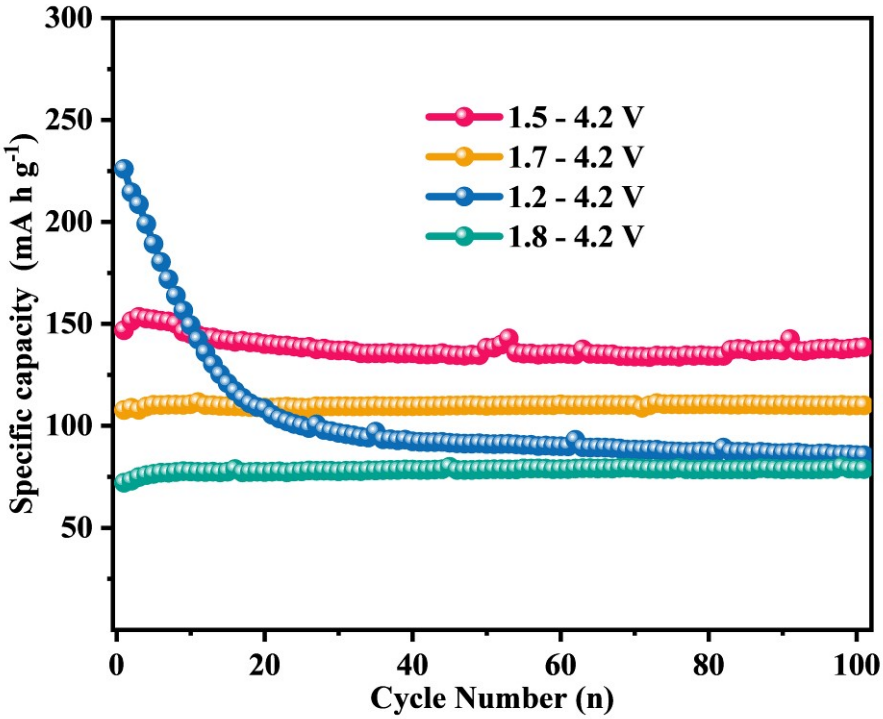

Fig. S9. Cycling performance at different voltage ranges of TPPDA-CuPor-COF.

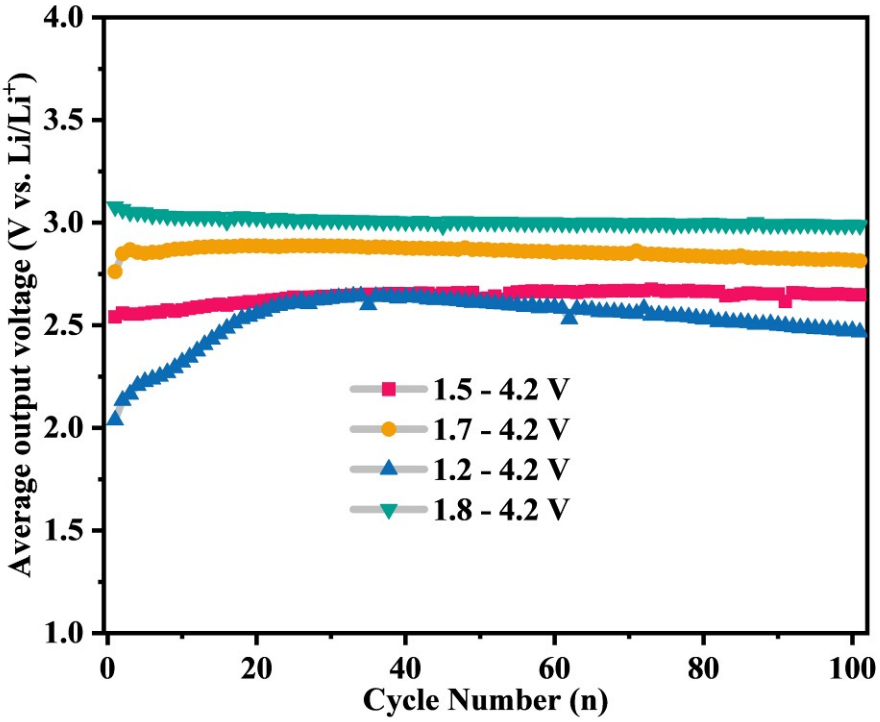

Fig. S10. The average output voltages at different voltage ranges of TPPDA-CuPor-COF.

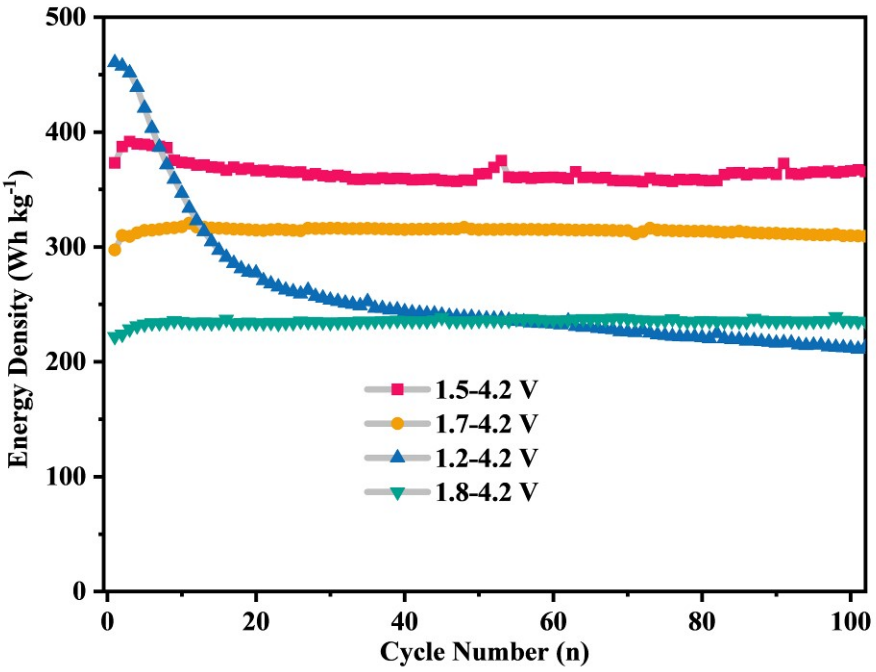

Fig. S11. Energy densities of TPPDA-CuPor-COF under different voltage ranges.

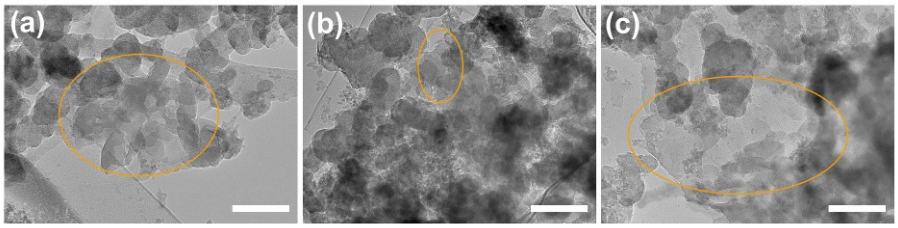

Fig. S12. The TEM images (scale bar = 100 nm) of TPPDA-CuPor-COF electrode: (a) pristine, (b) charged to 4.2 V and (c) discharged to 1.5 V.

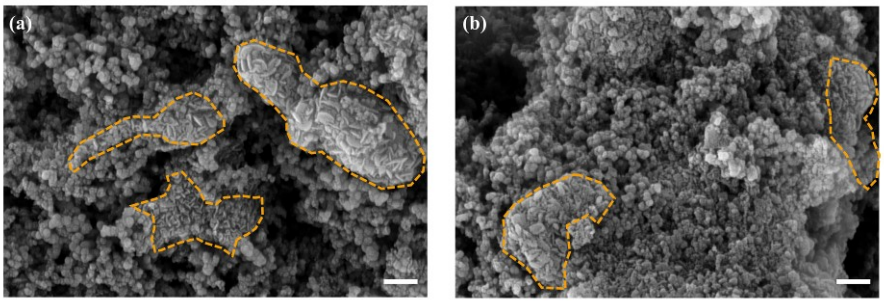

Fig. S13. The SEM images of TPPDA-CuPor-COF electrode :(a) pristine and (b) after 50 cycles of charge-discharge (scale bar = 300 nm).

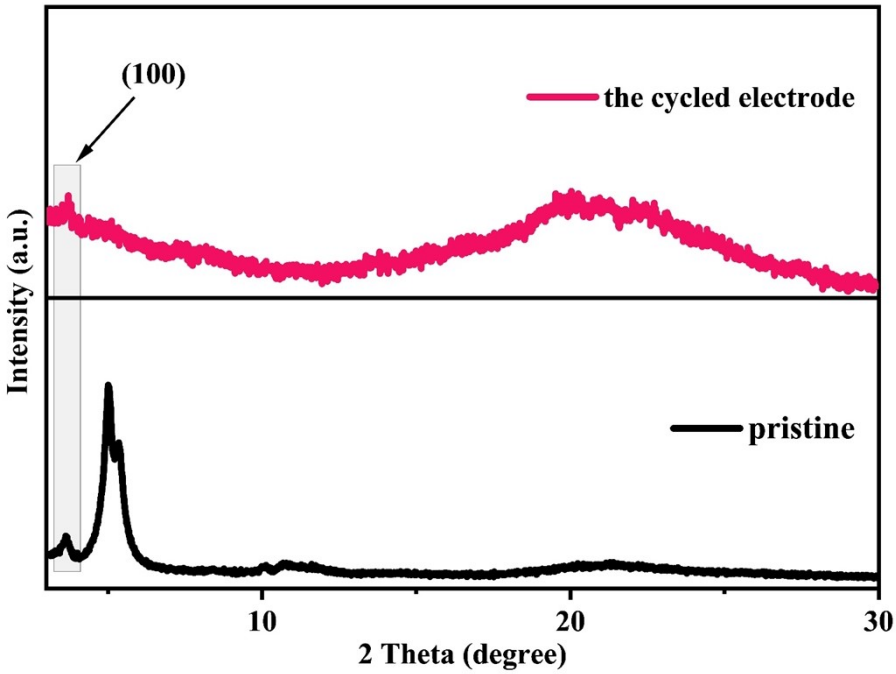

Fig. S14. The *ex*-situ XRD diagram of TPPDA-CuPor-COF cathode after 50 cycles of charge-discharge.

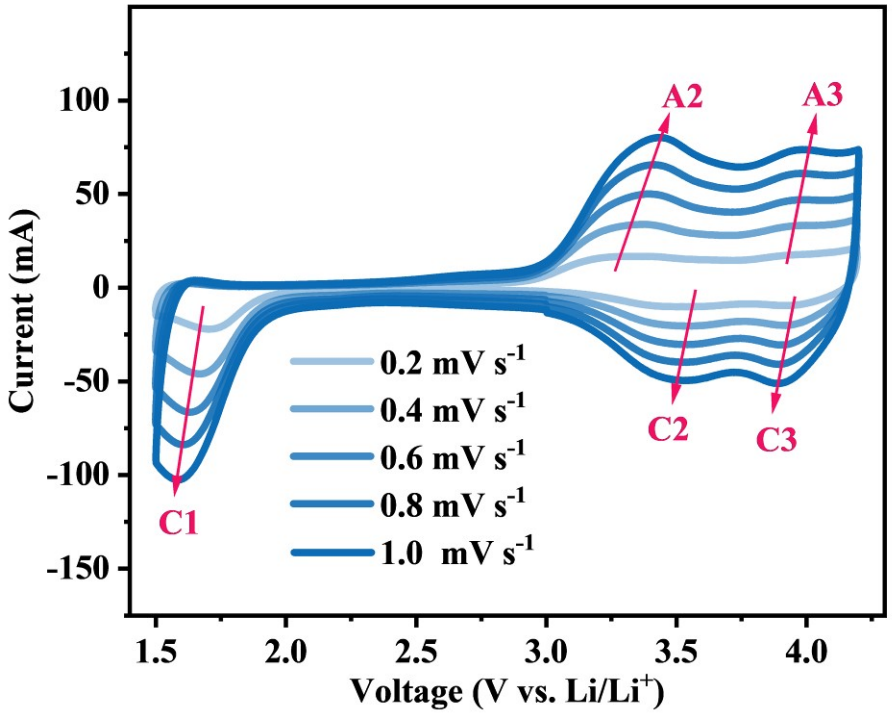

Fig. S15. The CV curves at different scan rates.

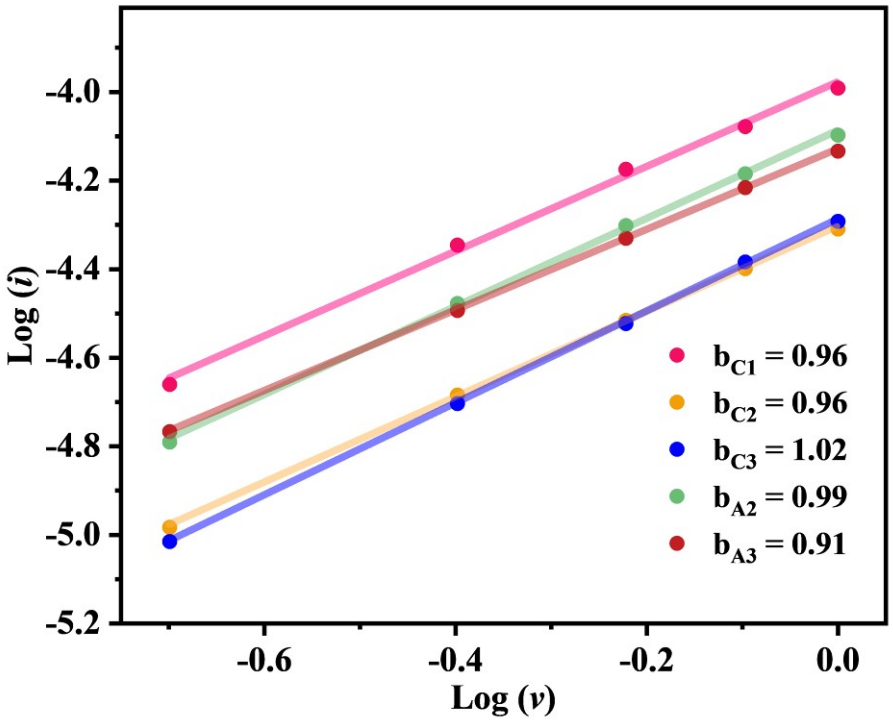

Fig. S16. The corresponding plots of log(*i*) versus log(*v*) at each redox peak.

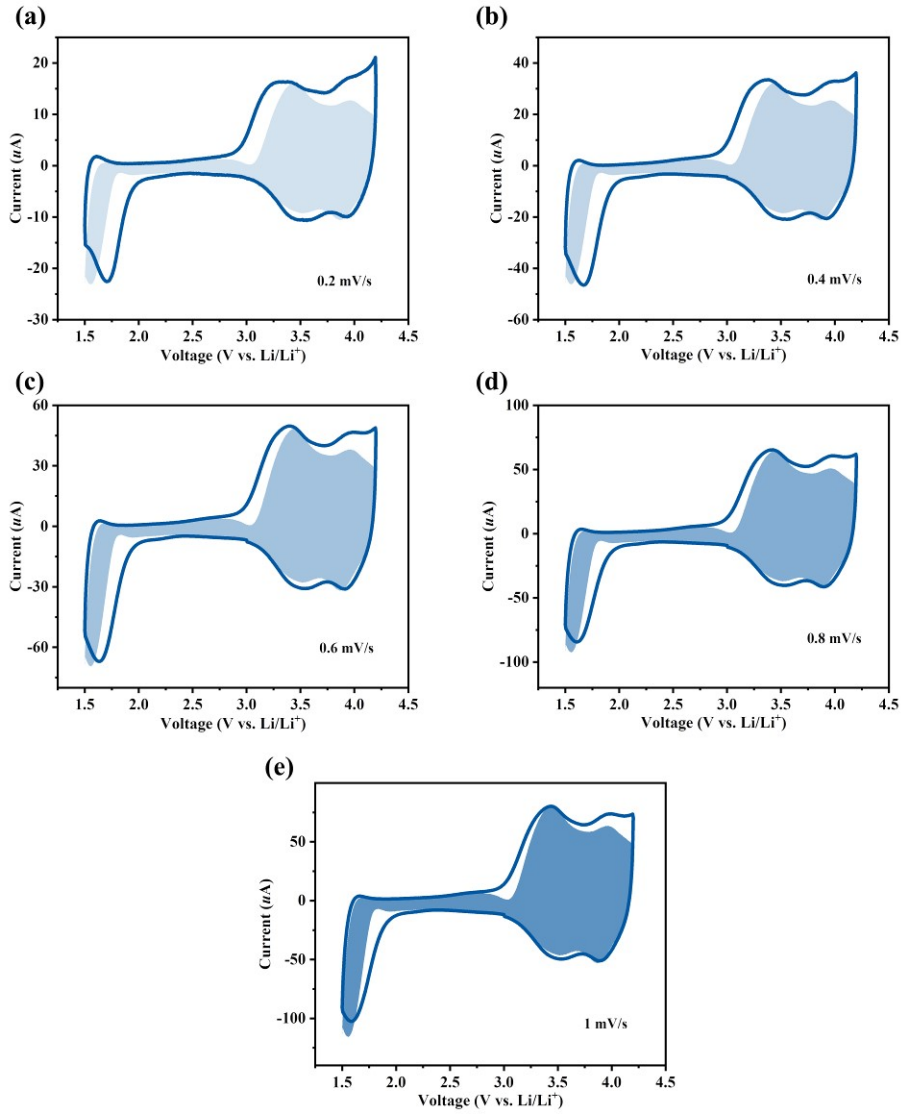

Fig. S17. CV profiles and pseudocapacitive contributions (blue shadow) at different scan rates of TPPDA-CuPor-COF.

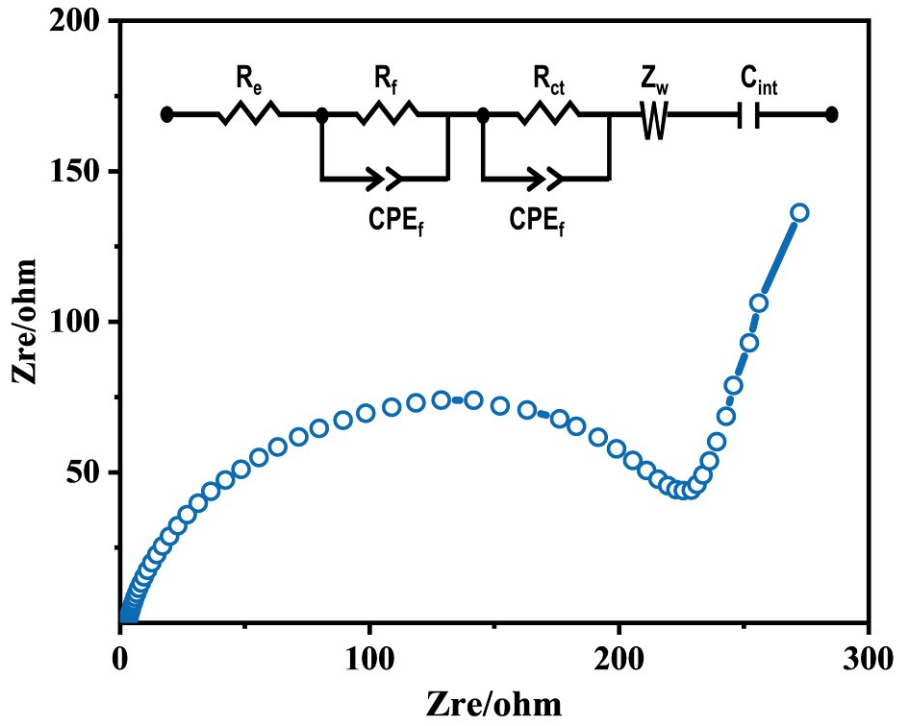

Fig. S18. The Nyquist plots and simulated equivalent circuit of the electrode/electrolyte interface.

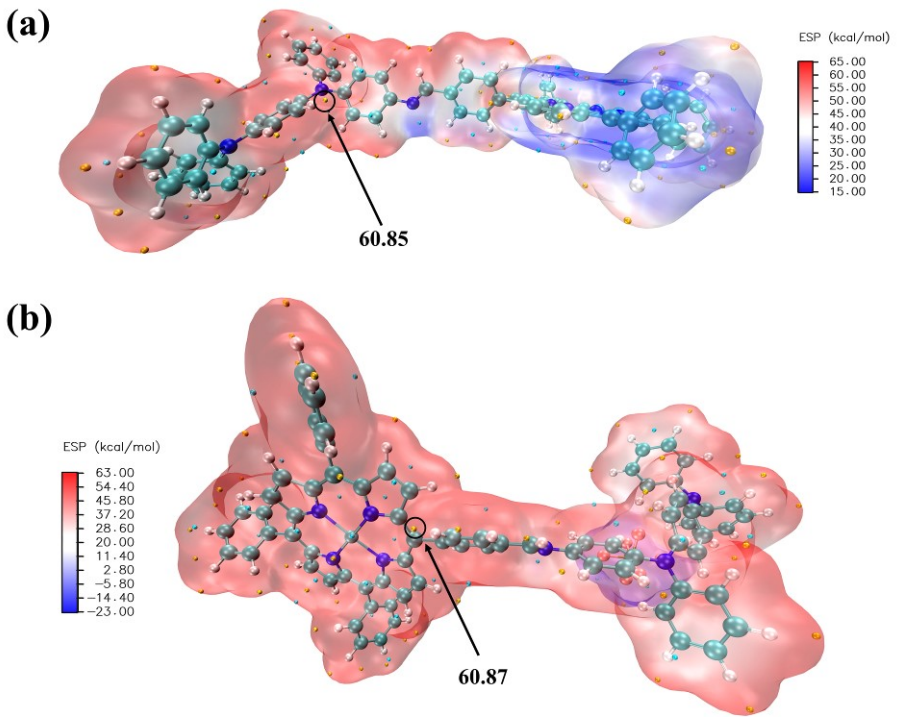

Fig. S19. (a) The MESP mapping image of $[TPPDA\text{-}CuPor]^{+}$, **(b)** the MESP mapping image of $[TPPDA\text{-}CuPor]^{2+}\bullet PF_6^{-}$.

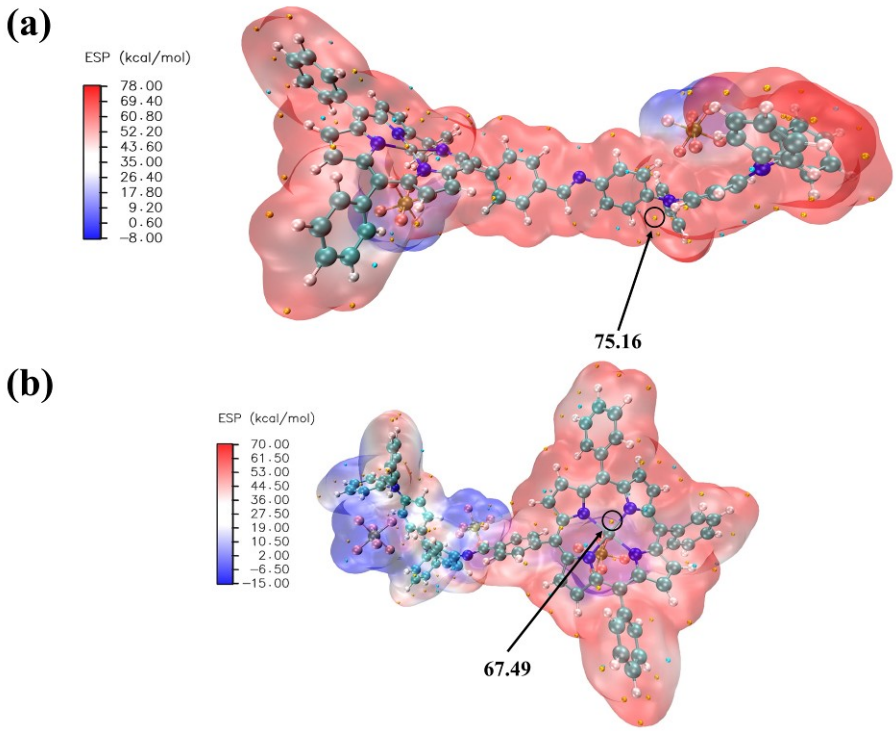

Fig. S20. (a) The MESP mapping image of $[TPPDA\text{-}CuPor]^{3+}\bullet 2PF_6^-$, **(b)** the MESP mapping image of $[TPPDA\text{-}CuPor]^{4+}\bullet 3PF_6^-$.

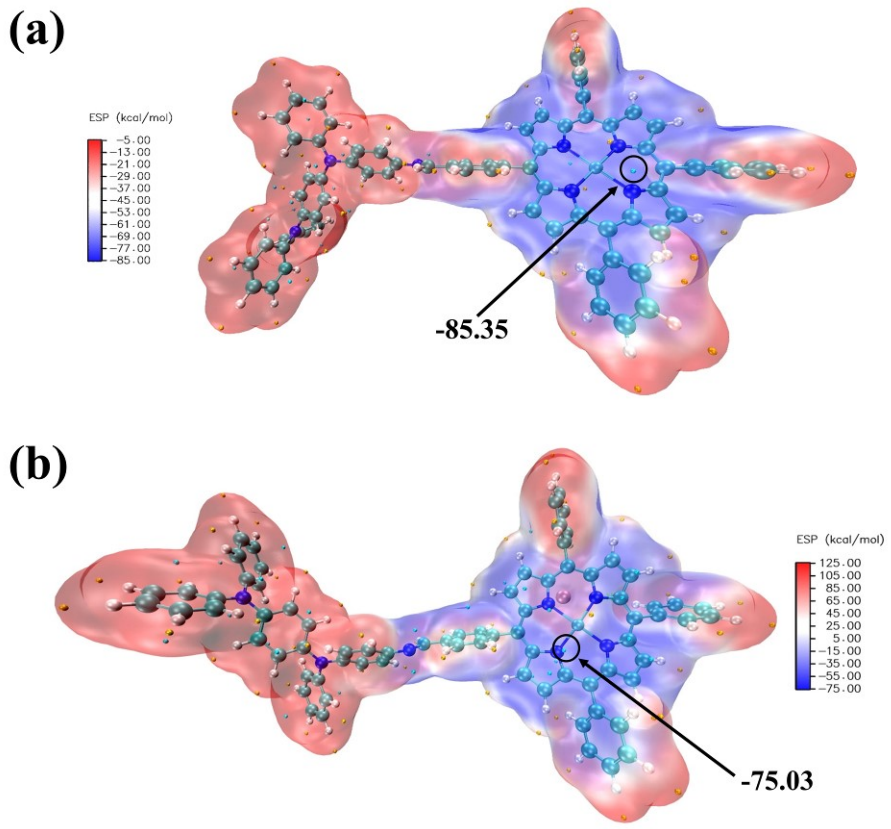

Fig. S21. (a) The MESP mapping image of TPPDA-CuPor $^{-}$, **(b)** the MESP mapping image of $[TPPDA\text{-}CuPor]^{2-}\bullet Li^{+}$.

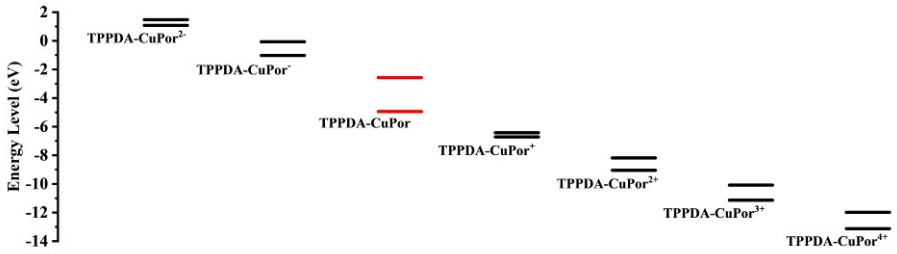

Fig. S22. The energies of the HOMO and LUMO of TPPDA-CuPor under different redox states.

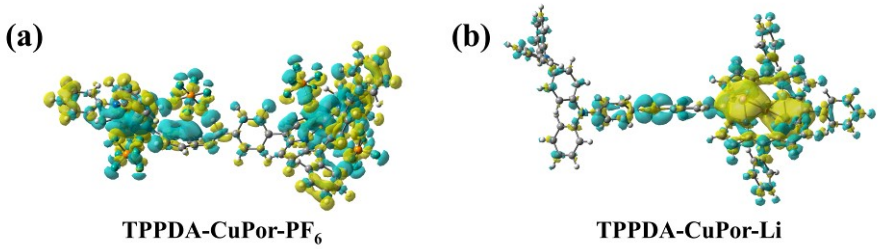

Fig. S23. The differential charge analyses between TPPDA-CuPor and charge carriers (the yellow region: charge density increased; the cyan region: charge density decreased).

Table S1. The metal content of TPPDA-CuPor-COF calculated from ICP tests.

Sample	Calculated (wt%)	Found (wt%)
TPPDA-CuPor-COF	5.33	5.18

Table S2. Comparison of organic p- and bipolar-type cathode materials in Lithium-ion battery.

Materials	The voltage region of discharge (V)	Current density, discharge capacity (mA h g^{-1})	Current density, cycles, capacity retention	Reference
PTPAn	4.2-3.0	0.5C 103	20C 1000th, 87%	J. Power Sources 177 (2008) 199-204.
3PXZ	4.0-3.0	1C 112	1C 100th, 65%	Energy. Environ. Sci., 13 (2020) 4142-4156.
3PTZ	4.0-3.0	1C 31	1C 100th, 66%	
PVK	4.7-2.0	20 mA g^{-1} 120	20 mA g^{-1} 50th, 97%	J. Power Sources 202 (2012) 364-368.
P1	4.4-3.3	1C 66	1C, 100th, 32%	Chem. Commun. 51 (2015) 15261-15264.
TCTA	4.7-3.0	1 A g^{-1} 92	1 A g^{-1} 5000th 60%	Angew. Chem. Int. Ed. 132 (2020) 12090-12096.
DAPO-TFB-COF	4.2-1.5	100 mA g^{-1} 66.8	100 mA g^{-1}, 1000th, 72%	J. Mater. Chem. A 9 (2021) 10661-10665.
DAPO-TpOMe-	4.2-1.5	100 mA g^{-1}	100 mA g^{-1}, 1000th,	

COF		80.0	85%	
p-DPPZS	4.5-2.5	147 mA g^{-1} 126	735mA g^{-1}, 1000th, 90%	Matter, 1 (2019) 945-958.
poly(S-TTN)	4.4-2.8	1C 122	5C, 180th, 90%	J. Electrochem. Soc. 157 (2010) F23.
X-PVMPT	3.9-3.1	1C 107	1C, 1000th, 95%	Adv. Energy Mater. 8 (2018) 1802151.
PDDP	4.2-2.5	20 mA g^{-1} 129.1	20 mA g^{-1}, 50th, 86%	J. Mater. Chem. A 2 (2014) 20083-20088.
PTPA	4.2-2.5	20 mA g^{-1} 94.7	20 mA g^{-1}, 50th, 89%	
TEMPO-COF	4.1-2.0	20 mA g^{-1} 75	*	J. Am. Chem. Soc. 139 (2017) 4258-4261.
TEMPO-ECOF	4.1-2.0	20 mA g^{-1} 115	*	
poly-PPDA-PYR	4.2-2.0	20 mA g^{-1} 113	500 mA g^{-1}, 600th, 80%	Chem. Asian J. 14 (2019) 2210-2214.
TPPDA-CuPor-COF	4.2-1.5	60 mA g^{-1} 142	1000 mA g^{-1}, 3000th, 86%	**This work**

(*: not provided.)

Table S3. The EIS data of the TPPDA-CuPor-COF cathode.

TPPDA-CuPor-COF	Values	Fitting Error (%)
R_e (Ω)	3.5	3.41
R_f (Ω)	151.2	3.27
R_{ct} (Ω)	37.8	7.49
Sum (Ω)	192.5	-

REFERENCES

(1) S. Muench, A. Wild, C. Friebe, B. Häupler, T. Janoschka, U.S. Schubert, *Chem. Rev.*, 2016, **116**, 9438-9484.

(2) W. Yang, R.G. Parr, C. Lee, *Physical Review B,* 1988, **37**, 785-789.

(3) S. Grimme, J. Antony, S. Ehrlich, H. Krieg, *J. Phys. Chem. B*, 2010, **132**, 154104.

(4) B.P. Pritchard, D. Altarawy, B. Didier, T.D. Gibson, T.L. Windus, J. Chem. *Inf. Model.*, 2019, **59**, 4814-4820.

(5) M. J. Frisch, G. W. Trucks, H. B. Schlegel, G. E. Scuseria, M. A. Robb, J. R. Cheeseman, G. Scalmani, V. Barone, B. Mennucci, G. A. Petersson, H. Nakatsuji, M. Caricato, X. Li, H. P. Hratchian, A. F. Izmaylov, J. Bloino, G. Zheng, J. L. Sonnenberg, M. Hada, M. Ehara, K. Toyota, R. Fukuda, J. Hasegawa, M. Ishida, T. Nakajima, Y. Honda, O. Kitao, H. Nakai, T. Vreven, J. A. Montgomery, Jr., J. E. Peralta, F. Ogliaro, M. Bearpark, J. J. Heyd, E. Brothers, K. N. Kudin, V. N. Staroverov, T. Keith, R. Kobayashi, J. Normand, K. Raghavachari, A. Rendell, J. C. Burant, S. S. Iyengar, J. Tomasi, M. Cossi, N. Rega, J. M. Millam, M. Klene, J. E. Knox, J. B. Cross, V. Bakken, C. Adamo, J. Jaramillo, R. Gomperts, R. E. Stratmann, O. Yazyev, A. J. Austin, R. Cammi, C. Pomelli, J. W. Ochterski, R. L. Martin, K. Morokuma, V. G. Zakrzewski, G. A. Voth, P. Salvador, J. J. Dannenberg, S. Dapprich, A. D. Daniels, O. Farkas, J. B. Foresman, J. V. Ortiz, J. Cioslowski, and D. J. Fox, Gaussian 09, Version D.01, Gaussian, Inc., Wallingford CT, 2013.

(6) T. Lu, F. Chen, *J. Comput. Chem.,* 2012, **33**, 580-592.

(7) W. Humphrey, A. Dalke and K. Schulten, *J Mol Graph*, 1996, **14**, 33-38, 27-28.

(8) H. Zhang, R. Zhang, X. Liu, F. Ding, C. Shi, Z. Zhou, N. Zhao, *J. Mater. Chem. A*, 2021, **9**, 24915-24921.